

## Multitone Microwave Frequency Locking to a Noisy Cavity via Real-Time Feedback

Van Soest, J. P.; Potts, C. A.; Peiter, S.; Sanz Mora, A.; Steele, G. A.

**DOI**

[10.1103/PhysRevApplied.20.034007](https://doi.org/10.1103/PhysRevApplied.20.034007)

**Publication date**

2023

**Document Version**

Final published version

**Published in**

Physical Review Applied

**Citation (APA)**

Van Soest, J. P., Potts, C. A., Peiter, S., Sanz Mora, A., & Steele, G. A. (2023). Multitone Microwave Frequency Locking to a Noisy Cavity via Real-Time Feedback. *Physical Review Applied*, 20(3), Article 034007. <https://doi.org/10.1103/PhysRevApplied.20.034007>

**Important note**

To cite this publication, please use the final published version (if applicable). Please check the document version above.

**Copyright**

Other than for strictly personal use, it is not permitted to download, forward or distribute the text or part of it, without the consent of the author(s) and/or copyright holder(s), unless the work is under an open content license such as Creative Commons.


**Takedown policy**

Please contact us and provide details if you believe this document breaches copyrights. We will remove access to the work immediately and investigate your claim.

# Multitone Microwave Frequency Locking to a Noisy Cavity via Real-Time Feedback

J.P. van Soest<sup>✉,\*</sup>, C.A. Potts<sup>✉</sup>, S. Peiter, A. Sanz Mora, and G.A. Steele<sup>✉,†</sup>

*Kavli Institute of NanoScience, Delft University of Technology, P.O. Box 5046, Delft 2600 GA, Netherlands*

 (Received 6 April 2023; revised 12 July 2023; accepted 7 August 2023; published 6 September 2023)

Microwave cavities are commonly used in many experiments, including optomechanics, magnetic field sensing, magnomechanics, and circuit quantum electrodynamics. Noise, such as variations in the magnetic field or mechanical vibrations, can cause fluctuations of the natural frequency of the cavity, creating challenges in operating them in experiments. To overcome these challenges, we demonstrate a dynamic feedback system implemented by the locking of a microwave drive to the noisy cavity. A homodyne-interferometer scheme monitors the cavity resonance fluctuations due to low-frequency noise, which is mitigated by frequency modulating the microwave generator. The feedback has a bandwidth of 400 Hz, with a reduction of cavity fluctuations by 85% integrating up to a bandwidth of 2 kHz. Moreover, the cavity resonance frequency fluctuations are reduced by 73%. This scheme can be scaled to enable multitone experiments locked to the same feedback signal. As a demonstration, we apply the feedback to an optomechanical experiment and implement a cavity-locked multitone mechanical measurement. As low-frequency cavity frequency noise can be a limiting factor in many experiments, the multitone microwave locking technique presented here is expected to be relevant for a wide range of microwave-cavity experiments.

DOI: [10.1103/PhysRevApplied.20.034007](https://doi.org/10.1103/PhysRevApplied.20.034007)

## I. INTRODUCTION

Low-frequency noise is often the limiting factor in mechanical and magnetic experiments [1–9], arising from, e.g., variations in the magnetic field or vibrations in cryogenic experiments. These sources of noise can cause fluctuations in the resonance of a microwave cavity. There are two common ways to counteract this noise: the first is to dampen the noise before it reaches the device under test. While a mass-on-a-spring low-pass filter can suppress high-frequency vibrations for mechanical experiments [10,11], the lowest frequencies can often introduce considerable noise. In this sense, the mechanical filter is not optimal: it is effective at blocking high frequencies but not low frequencies. The second method actively counters noise by applying dynamic feedback to the system [12,13]. As a feedback system is limited by its feedback bandwidth and response time, it acts as a high-pass filter: it cannot react at high frequencies but is very effective at low frequencies. Combining these two complementary techniques, therefore, gives an opportunity for noise reduction over the entire spectrum.

In this work, we present an active feedback system based on the cavity-stabilization method introduced by

Pound in Ref. [14]. Here, the inverse of the Pound-Drever-Hall technique [15–18] is applied using active feedback to adjust a microwave generator frequency, locking it to a cavity the resonance frequency of which fluctuates in time. This scheme not only locks a single microwave signal to the cavity but also enables the active locking of multiple tones using the same feedback signal, demonstrated in Sec. V.

Since any source of low-frequency cavity noise can be mitigated, this technique has applications in various fields. It can be used to modulate magnetic flux to stabilize superconducting quantum interference device (SQUID) cavities [13,19] and magnomechanical experiments [20–23], which are also known to suffer from magnetic field noise. As we demonstrate in Sec. VI, our technique can be directly applied to an optomechanical system experiencing mechanical noise [24]. As identified in previous work, cavity frequency noise from vibrations can be a limiting factor in the ground-state cooling of mechanical resonators [25].

## II. EXPERIMENTAL SETUP

To demonstrate the feedback system, we apply it to a radio-frequency (rf) circuit in an optomechanical flip-chip setup, similar to Refs. [26,27]. The microwave cavity consists of a meander inductor  $L$  and a pair of capacitor plates  $C_0$  etched into a Nb-Ti-N film, approximately 1  $\mu\text{m}$  above which a mechanically compliant capacitor

\*j.vansoest-1@tudelft.nl

†g.a.steele@tudelft.nl

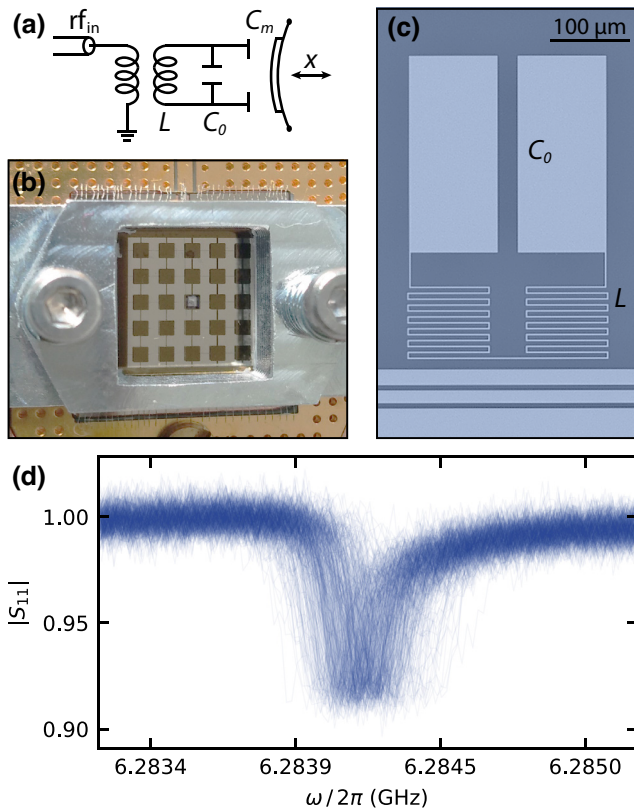


FIG. 1. A microwave cavity with resonance-frequency fluctuations. (a) A lumped-element-circuit schematic of the device under test. (b) An optical image of the flip-chip device. The metallized membrane can be seen as a white square in the phononic shield. (c) An optical micrograph of the rf circuit. The meander inductor  $L$  and capacitor  $C_0$  form the microwave cavity. (d) 500 individual normalized 240- $\mu$ s vector network analyzer (VNA) traces show a distribution of the cavity resonance frequency  $\omega_c$ .

$C_m$  is positioned. A circuit schematic of the device and optical images are shown in Figs. 1(a)–1(c). The top capacitor plate consists of aluminum deposited on a thin silicon nitride membrane, embedded within a patterned silicon substrate etched to form a phononic shield (see, e.g., Refs. [27,28]). The primary purpose of the phononic crystal structure is to reduce unwanted mechanical noise at 1 MHz and to suppress the radiative loss of mechanical energy through the substrate, as shown in Ref. [25]. However, the phononic crystal has the unwanted side effect of increasing the mechanical susceptibility of the top chip to low-frequency (approximately kilohertz) vibrations in the setup [29].

The resonance frequency of the flip-chip cavity is given by  $\omega_c(t) = [L(C_0 + C_m(t))]^{-1/2} \approx 2\pi \times 6.28$  GHz. Vibrations drive low-frequency modes of the top chip, resulting in a time-dependent capacitance  $C_m(t)$ . Therefore, these low-frequency mechanical vibrations of the top chip modulate the cavity resonance frequency  $\omega_c$ . The fluctuations in the cavity resonance frequency can be seen in Fig. 1(d),

where many repeated vector network analyzer (VNA) sweeps demonstrate the noise imparted on the microwave resonator. These measurements have been performed on the base plate of a dilution refrigerator held at approximately 20 mK. The pulse-tube cooler is the primary source of vibrations within a dry dilution refrigerator; therefore, the pulse tube was switched off during measurements to reduce vibrations within the experimental setup. However, we have still observed that the resonance-frequency fluctuations are on the order of the linewidth of the cavity. To compensate for these fluctuations, we have implemented an active feedback system to track the resonance frequency of the cavity.

### III. FEEDBACK SYSTEM

To compensate for the fluctuating cavity frequency, we have developed a feedback system similar to the Pound-Drever-Hall technique [15–18]. While the Pound-Drever-Hall technique is usually used to stabilize a noisy laser by locking it to a stable optical cavity, here we apply its inverse role: we lock a stable generator to the resonance frequency of a noisy cavity. In our system, the microwave frequency of the drive tone is locked to the fluctuating resonance frequency of the cavity. Locking the drive tone is accomplished by producing an error signal depending on the time-dependent resonance frequency of the cavity. The error signal is then used in an active feedback loop to frequency modulate the output of the microwave generator, producing a drive tone that tracks the shifting cavity resonance frequency. A schematic diagram of the feedback system is shown in Fig. 2(a).

The scheme starts by splitting the local oscillator signal into two paths. One of them goes directly to the microwave cavity and is then directed into the rf port of a mixer. The other path goes through a path-length-matched reference arm to the local-oscillator (LO) port of the same mixer, making the system a balanced homodyne microwave interferometer. Small fluctuations in the resonance frequency of the microwave cavity result in a linear response at the output of the mixer, as seen in Fig. 2(b). This down-converted homodyne signal, which we call the homodyne voltage  $V_h$ , depends on the detuning of the cavity resonance frequency relative to the current microwave drive frequency. When the system is unlocked, the homodyne voltage fluctuations follow the fluctuations in the resonance frequency of the cavity. In this experiment, the cavity fluctuations are larger than the linear region of the homodyne down-converted signal. Thus, the local oscillator frequency is updated in real time by modulation using a control voltage  $V_c$  to track the cavity resonance frequency.

Sweeping the frequency  $\omega_{LO}$  of the local oscillator, a linear dependency between the control voltage  $V_c$  and the measured homodyne voltage  $V_h$  was observed around the

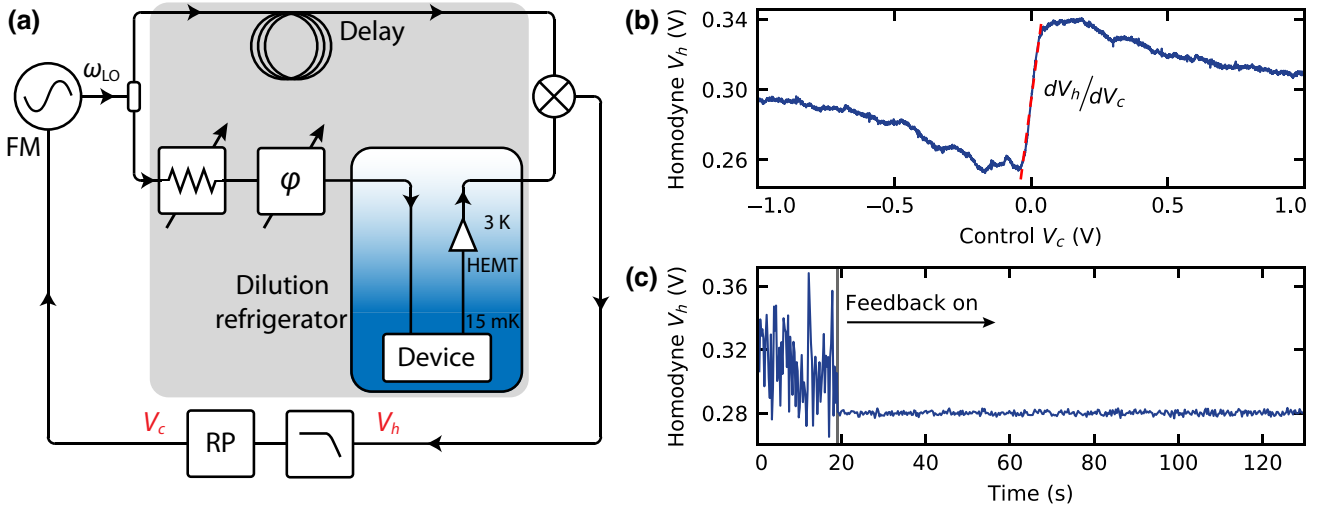


FIG. 2. The feedback system is used to reduce the cavity resonance frequency fluctuations. (a) A schematic of the feedback circuit, consisting of a balanced microwave homodyne interferometer, one path of which goes to the device under test. The reference arm is path-length matched, down-converting the signal at a mixer. The resulting voltage  $V_h$  is led to a Red Pitaya (RP), which creates a control voltage  $V_c$  to frequency modulate (FM) the local oscillator  $\omega_{LO}$ . (b) The homodyne response as the control voltage  $V_c$  sweeps the local oscillator frequency over the cavity resonance. Within the linewidth of the cavity, the response is linear. Low-frequency noise can be seen outside the linear regime. (c) A time trace of the homodyne voltage  $V_h$ . The feedback is turned on at  $t = 19$  s.

cavity resonance, as seen in Fig. 2(b). Note that if an unbalanced homodyne detection scheme was used, the path-length difference would result in phase-winding fringes in the homodyne voltage signal, which could result in a loss of cavity lock. Thus, the use of a balanced homodyne scheme ensures a frequency-independent homodyne voltage signal regardless of the instantaneous local oscillator frequency (see Appendix A).

To maintain constant power arriving at the LO port of the mixer while having dynamic control over the power incident on the microwave resonator under test, a variable attenuator was added to the device arm. Moreover, the phase difference between the local oscillator and device arm was set to  $90^\circ$  out of phase, so that the quadrature signal was measured. The homodyne voltage is then low-pass filtered and led to a proportional-integral (PI) controller programmed in the field-programmable gate array (FPGA) of a Red Pitaya [30]. The output control voltage of the PI controller  $V_c$  continuously modulates the frequency  $\omega_{LO}$  of the local oscillator to remain resonant with the cavity frequency  $\omega_c$ . Ideally, the homodyne voltage is zero at resonance; however, a slight dc offset was present in the experiment, which determined the set point in the PI controller.

To optimize our feedback system, the proportional and integral gain of the PI controller needed to be tuned for optimal noise suppression. As the gain is increased, low-frequency noise is suppressed; however, a too-aggressive PI setting results in added noise at higher frequencies. The optimal value for all experimental implementations of our feedback system depends on the specific

configuration; therefore, each system must be calibrated to find the optimal PI gains. Turning on the feedback system stabilizes the homodyne voltage, as can be seen in Fig. 2(c). It should be noted that the feedback did not lose the lock during the measurements over a time of approximately 7 min (the period during which the pulse tube could be turned off).

#### IV. NOISE REDUCTION

We can quantitatively analyze the suppressed frequency noise in the reference frame of the cavity by considering the power spectral density of frequency fluctuations,  $S_{f/f_0}(f)$  ( $\text{Hz}^2/\text{Hz}$ ) [29]. The power spectral density can be calculated by taking the Fourier transform of the measured homodyne voltage  $V_h$  and is shown in Fig. 3(a). The power spectral density of the locked homodyne voltage,  $S_{V_h V_h}(f)$  ( $\text{V}^2/\text{Hz}$ ), was calibrated using the slope of the homodyne voltage versus the control voltage, shown in Fig. 2(b). However, the power spectral density of the unlocked homodyne signal cannot be calibrated in this way, since the region of linear response is narrower than the fluctuations of the cavity resonance frequency. Therefore, the detected homodyne signal does not contain information about large frequency fluctuations. An extra calibration has been applied to the unlocked spectra, as discussed in Appendix B.

We find that when we turn the feedback on, even with a small gain, the large frequency shifts of the cavity are compensated for and the cavity fluctuations remain within

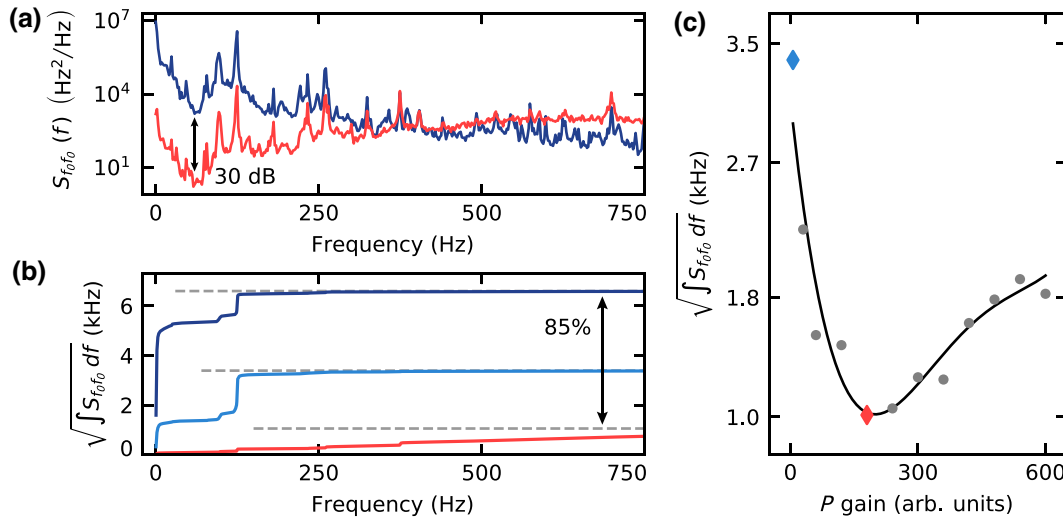


FIG. 3. The noise reduction of the homodyne voltage  $V_h$  depending on the feedback gain. (a) The power spectral density  $S_{f_{of0}}$  of the homodyne voltage  $V_h$  with the feedback off (dark blue) and on (red). The unlocked data has been calibrated as described in Appendix B. Noise is reduced up to 30 dB over a bandwidth of 400 Hz. (b) The integrated power spectral density for an unlocked (dark blue) and a locked cavity for two proportional and integral (PI) gains of the feedback loop (light blue and red). Asymptotes up to 2 kHz (dashed gray) show a noise reduction of 85%. (c) The integrated power spectral density up to 2 kHz for different PI gains of the feedback loop, using the same color coding. The solid black line is a polynomial fit to guide the eye.

the linear regime of the homodyne signal. This indicates that low-frequency fluctuations dominate the cavity noise. We have identified that for our system, the optimal proportional and integral gain ratio is  $P:I = 6:10$ . Figure 3(a) shows the power spectral density of the cavity unlocked and locked with the optimal feedback loop gain. It can be seen that for low frequencies, the noise is suppressed up to 30 dB. The spectra cross around 400 Hz, indicating the feedback bandwidth. Above this frequency, the system adds noise to the measurement, due to feedback of the added noise by the amplification chain used. At 2 kHz and above, the two spectra overlap, suggesting that no additional high-frequency noise is being added by our feedback system. Taking the square root of the integrated power spectral densities,  $S_{f_{of0}}(f)$ , we obtain the root-mean-square (rms) value for the noise power, in units of hertz. Even though there is added noise at intermediate frequencies, in Fig. 3(b) it can be seen that the total frequency noise is reduced. The integrated spectra show a noise reduction of 85% at 2 kHz, as indicated by the asymptotes shown in Fig. 3(b). Again, this suggests that low-frequency fluctuations were most detrimental in our system. Since the feedback loop acts as a high-pass filter, these low frequencies are compensated most efficiently.

Finally, the total gain of the feedback loop was varied by increasing the PI gain while keeping their ratio the same. Increasing the gain initially results in additional noise suppression until the feedback increases the total noise power, as shown in Fig. 3(c). This provides an optimal feedback loop gain for this system.

## V. MULTITONE LOCKING

Thus far, all measurements have been done using a single tone on cavity resonance. However, many experiments require multiple tones or, in fact, frequency sweeps. Since the local oscillator follows the resonance frequency of the cavity, the feedback circuit can easily be scaled up by adding additional generators to the same feedback setup. For example, an extra stage of up- and down-conversion was added to the circuit, as shown in Fig. 4(a). The gray box corresponds with that shown in Fig. 2(a). The local oscillator signal is now split into three paths: two paths in parallel are up-converted, to a lock signal  $\omega_{\text{lock}} = \omega_c - \omega_{\text{LO}}$  and a probe signal  $\omega_{\text{probe}}$  generated by a VNA; the third path goes to the reference arm as before. The signal coming from the cavity is first down-converted using  $\omega_{\text{LO}}$ , producing two tones at  $\omega_{\text{lock}}$  and  $\omega_{\text{probe}}$ . The signal at  $\omega_{\text{probe}}$  can be measured by the VNA as long as  $\omega_{\text{lock}}$  is not within the intermediate-frequency bandwidth (IFBW) of the measurement. The other path (at  $\omega_{\text{lock}}$ ) is down-converted a second time to dc, resulting, as before, in a voltage containing the frequencies of the cavity resonance fluctuations. This signal will also contain fluctuations at the frequency  $\delta = \omega_{\text{probe}} - \omega_{\text{lock}}$ . If  $\delta$  is within the feedback bandwidth of the cavity lock, it will need to be filtered out so as not to modulate the local oscillator with this frequency. Again, the down-converted signal is then led to the Red Pitaya to generate an error signal to frequency modulate the local oscillator.

Figure 4(b) shows VNA measurements with the feedback off and on, where the same number of traces have



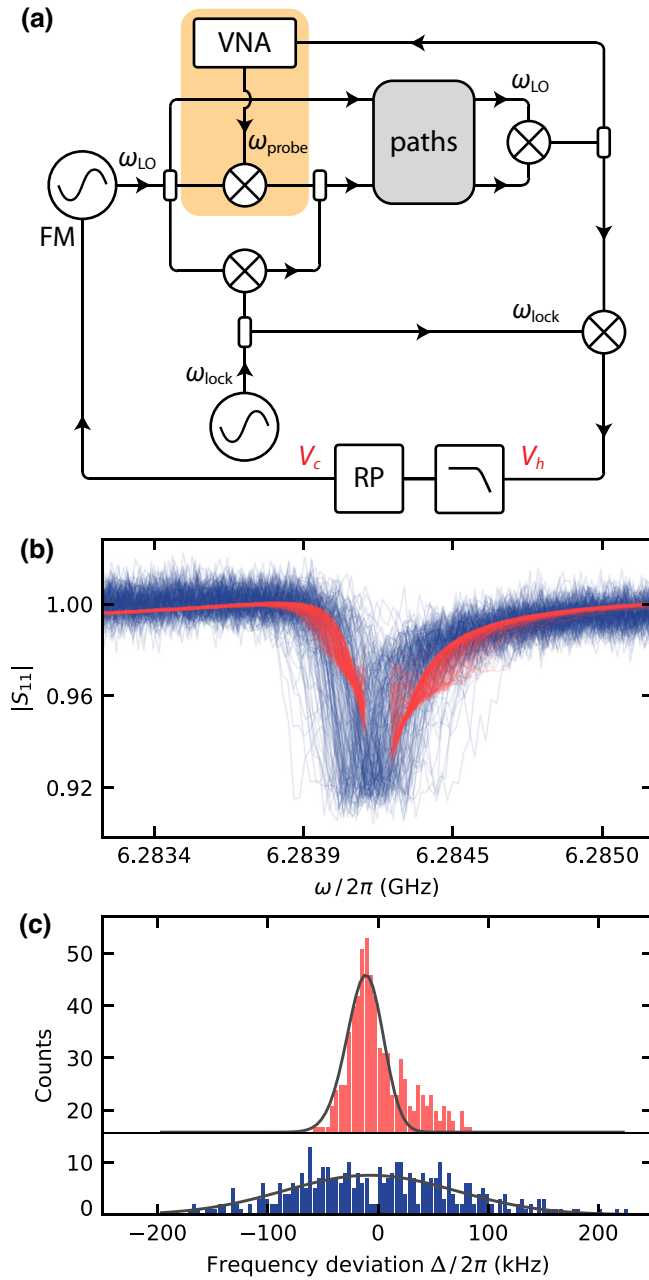


FIG. 4. The characterization of the locked-cavity response measured with the extended feedback circuit. (a) A schematic of the extended feedback circuit to lock multiple signals to the same feedback. The gray box corresponds with that in Fig. 2. The local oscillator is now up- and down-converted with a lock tone. The components in the orange box are included to add a probe tone to the input of the device. (b) Normalized VNA traces with the cavity unlocked (blue) and locked (red). Two separate measurements are performed for the locked cavity. (c) A histogram of the fitted resonance frequency of 376 traces unlocked and locked, using the same color coding. The locked histogram has been shifted for clarity. The standard deviation of the locked-cavity resonance frequency is  $\sigma_{\text{locked}} = 21$  kHz, which is a factor of 4 smaller than the unlocked  $\sigma_{\text{unlocked}} = 77$  kHz.

been used. Note that these measurements have been performed with an IFBW of 600 and 1 kHz, respectively, and with feedback gains of  $P = 480$  and  $I = 800$ . The locked measurement has been performed on the left and right sides of the cavity separately to avoid the lock tone entering the VNA measurement, as discussed above. However, if a measurement requires a VNA sweep on cavity resonance, it is also possible to lock off resonance (see Appendix A).

The individual traces have been fitted using a Lorentzian function to determine the resonance frequency for each trace. The extracted resonance frequencies of the unlocked and locked traces are compared in Fig. 4(c). The left and right data sets are fitted separately, using a fixed asymmetry due to the Fano effect [31] extracted from the unlocked measurement. Here,  $\Delta$  is the deviation from the average value of the fitted resonance frequency. The fits give skewed Gaussian distributions with a standard deviation  $\sigma_{\text{unlocked}} = 77$  kHz and  $\sigma_{\text{locked}} = 21$  kHz, which is a decrease of 73% for the locked measurement.

## VI. OPTOMECHANICAL EXPERIMENTAL VALIDATION

As a demonstration of the applicability of the feedback system, it is used in an optomechanical experiment [24]. The metal film of the capacitor  $C_m$  is located on a high-tensile-stress silicon nitride membrane, parametrically coupling the membrane to the cavity [26]. The membrane is isolated from its surroundings, as it is located in a phononic shield [25]. However, implementing this lattice structure also poses difficulties, as low-frequency modes are excited by vibrations in the dilution refrigerator. Although the energy of these lattice vibrations will mostly not be transferred to the vibrational mode of the membrane, it does mean that the membrane is located on a moving structure. As these modes alter the distance between the two chips by an amount larger than the amplitude of the vibrational mode of the membrane, this noise will change  $C_m$ , and thus also  $\omega_c$ , significantly.

As introduced in Sec. V, multiple microwave tones can be sent to the device while locked to the same local oscillator. Simply by multiplexing generators and mixers after the local oscillator, more drive frequencies can be added. Repeating the elements inside the orange box Fig. 4(a) offers continual scaling.

Figure 5(a) shows the scheme for a multitone measurement. By applying a drive tone detuned from the red sideband of the cavity,  $\omega_{\text{pump}} = \omega_c - \omega_m - \delta$ , and probing close to resonance,  $\omega_{\text{probe}} = \omega_c - \delta$ , the mechanical resonance appears from optomechanically induced transparency (OMIT) [32–34]. While having the local oscillator locked, a measurement of the mechanical resonance is presented in Fig. 5(b). Note that the asymmetry of the OMIT peak is due to the detuning  $\delta \approx 150$  kHz of the pump

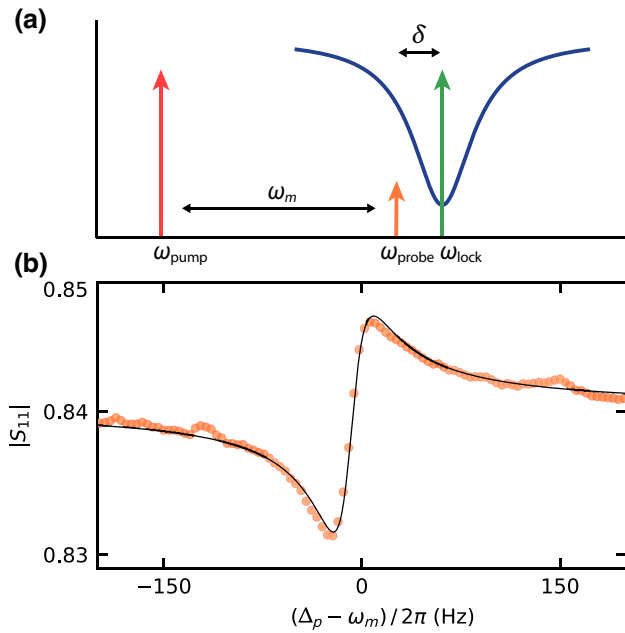


FIG. 5. A demonstration of a cavity-locked multitone optomechanical measurement. (a) An illustration of the driving scheme. The up-converted lock tone is set on the cavity resonance. The pump tone is applied  $\omega_m$  away from the center of the probe tone of the VNA, which in turn is detuned by  $\delta$  from resonance. (b) The mechanical resonance is visible as an optomechanically induced transparency (OMIT) peak, centered around  $\Delta_p = \omega_{\text{probe}} - \omega_{\text{pump}}$ , when the local oscillator is locked to the cavity, with  $\delta \approx 150$  kHz. Normalized data are shown in orange with a fit in black.

and probe with respect to the lock tone. However, it is equally possible to instead apply the detuning to the lock tone by adjusting the set point of the feedback circuit (see Appendix A).

## VII. CONCLUSIONS

In conclusion, we have presented a dynamic feedback system locking multiple microwave tones to an unstable microwave cavity. The frequency of a local oscillator has been modulated to follow the cavity resonance frequency by calibrating the homodyne signal to a control voltage. The power spectral density of the homodyne voltage has been analyzed, revealing a noise reduction of 85% at 2 kHz. Optimization of the feedback loop and the PI controller has resulted in an optimal response for our system, with a feedback bandwidth of 400 Hz. Furthermore, we have extended the feedback system to enable multitone experiments. Additional microwave tones have been implemented by up-conversion with the same locked tone of the local oscillator. Moreover, VNA measurements probing the cavity have shown that fluctuations in the cavity resonance frequency when locked have a standard deviation of  $\sigma_{\text{locked}} = 21$  kHz, as opposed to an

unlocked measurement with  $\sigma_{\text{unlocked}} = 77$  kHz, which is an improvement of 73%.

Finally, we have demonstrated the applicability of the feedback system by performing an optomechanical experiment. We have observed OMIT using another locked tone from a third generator without losing the cavity lock. Our feedback system provides continual scaling for adding tones to the same lock by multiplexing generators and mixers after the local oscillator. Besides optomechanics [35,36], the feedback system presented here has applications in various fields, as any source of low-frequency cavity noise can be reduced. For example, other potential applications include reducing two-level system noise [37] and locking to coplanar-waveguide resonators [38], SQUID cavities [19], gravitational-wave detectors [6], axion dark-matter detectors [39], and magnomechanical experiments [20–23].

The code and data necessary to produce the figures of the manuscript are uploaded to Zenodo [40].

## ACKNOWLEDGMENTS

This work was supported by the European Union Horizon 2020 research and innovation program under Grant Agreement No. 681476—QOM3D and the Dutch Research Council (NWO) through a Vici award from the NWO Talent Programme. C.A.P. acknowledges the support of the Natural Sciences and Engineering Research Council of Canada (NSERC).

## APPENDIX A: HOMODYNE PHASE MATCHING

It is worth discussing the effect of the balanced interferometer. As mentioned in Sec. III, the path length of the reference arm of the interferometer is matched to that of the signal arm. In contrast to the most common use of an interferometer, where the absolute phase difference of the two signals is not important, here we need to match the phases exactly. Because the noise in the system causes the resonance frequency of the cavity to fluctuate, our feedback system continually changes the frequency of the drive tone and, thereby, its wavelength. Therefore, the signals arriving at the mixer will have a frequency-dependent phase difference unless the two path lengths are identical.

Figure 6 shows the calculated homodyne voltage  $V_h$  for a balanced and a  $\Delta L = 10$  m unbalanced interferometer. In both cases, the incoming signals are set to be  $90^\circ$  out of phase, to measure the quadrature signal. It is clearly visible that in the unbalanced case, there is a sinusoidal profile superimposing the frequency response of the cavity, known as phase-winding fringes. The linear regime has decreased significantly, increasing the chance for the lock to fringe hop to the next slope. This would result in an unstable feedback signal.

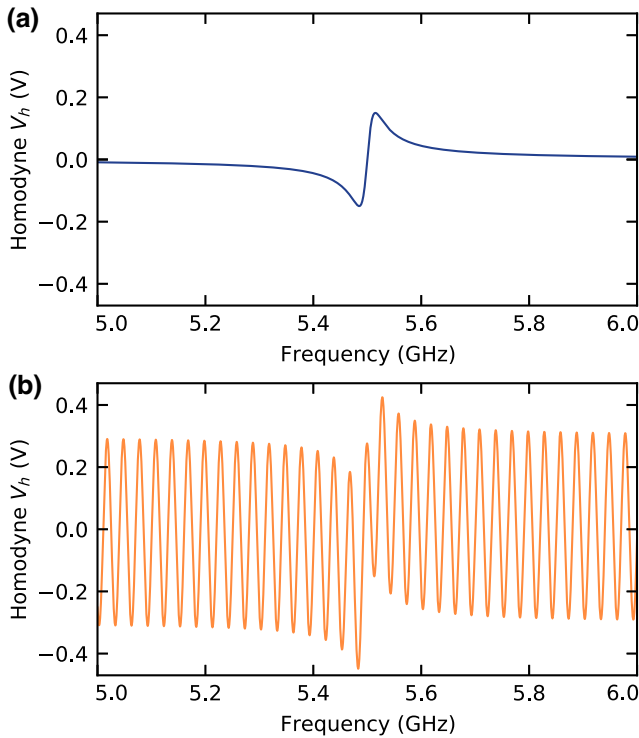


FIG. 6. The homodyne response for different interferometer path lengths. (a) The calculations for a balanced interferometer. (b) The calculations for an interferometer unbalanced by  $\Delta L = 10$  m.

Moreover, it is possible to send the lock tone off resonance from the cavity by adjusting the set point as long as the tone is within the linear regime of the homodyne response. However, one advantage of the homodyne voltage locking, in contrast to the conventional Pound-Drever-Hall technique [15–18], is that one can also

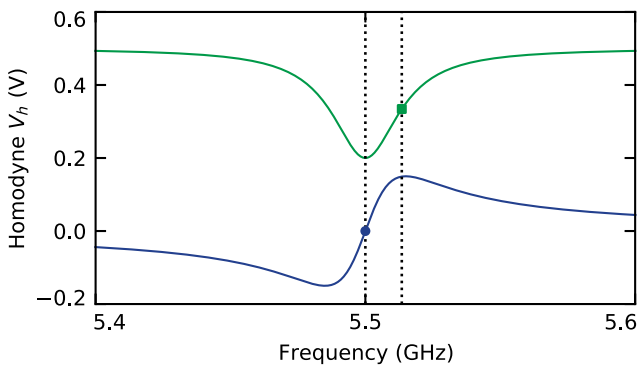


FIG. 7. The calculated homodyne response for two quadratures, as defined by the phase difference of the two signals coming into the mixer. Locking on resonance can be achieved using the “phase” quadrature (blue), with a tone resonant with the nominal cavity frequency and a feedback set point indicated by the blue circle. Locking off resonance can be achieved by choosing the orthogonal “amplitude” quadrature (green) and a set point indicated by the green square.

choose to lock at other points in the cavity. Doing so will sacrifice some stability, which will reduce the quality of the lock, but choosing the right phase difference at the mixer allows one lock on the other quadrature, as demonstrated in Fig. 7. The dashed lines show examples of set points that allow locking on and off resonance, while still remaining on an unidirectional slope, using the other quadrature. Note that moving the set point further from resonance can decrease the stability of the lock.

APPENDIX B: SPECTRAL-DENSITY CALIBRATION

The fluctuations of the unlocked-cavity resonance frequency were greater than the region of linear response of the homodyne voltage, as shown in Fig. 2(b). As a result, the measured homodyne voltage did contain information about large frequency fluctuations. To compare the unlocked and locked noise spectra, separate calibration measurements had to be performed. With the Red Pitaya,

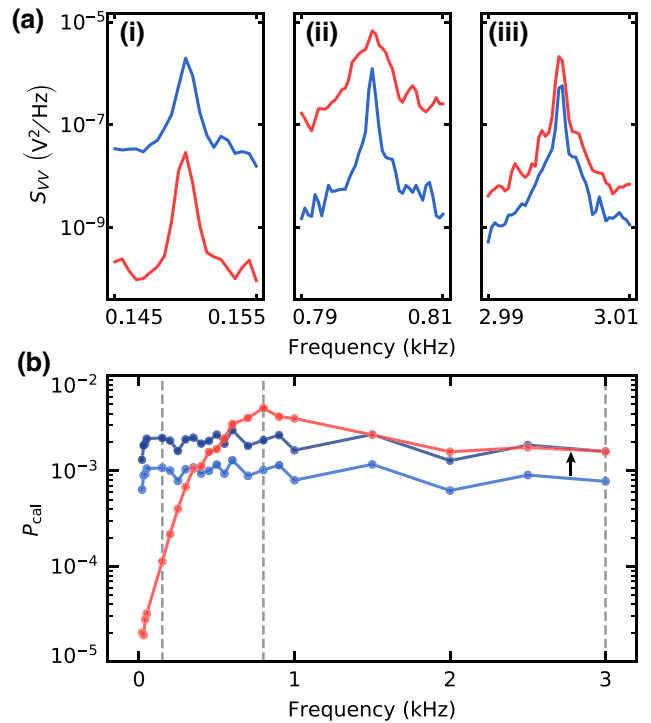


FIG. 8. The calibration of the unlocked power spectral density. (a) Three measured homodyne power spectral density peaks, produced by an additional modulation tone applied to the local oscillator, for the unlocked (light blue) and locked (red) cavity. The calibration tones have been provided at different frequencies inside and outside the feedback bandwidth. (b) The integrated power of the measured calibration tones (i)  $f_{\text{cal}} = 150$  Hz, (ii)  $f_{\text{cal}} = 800$  Hz, and (iii)  $f_{\text{cal}} = 3$  kHz, using the same color coding. The dashed lines show the frequencies of the peaks in (a). The unlocked trace is corrected (dark blue) with an offset of the calibration factor.



an additional modulation was applied to the local oscillator at different frequencies  $f_{\text{cal}}$  for both the unlocked and locked cavity. The amplitude of this tone caused a frequency fluctuation of the drive tone that was well within the linear regime of the locked homodyne response and resulted in a sharp peak in the measured power spectral density at the modulation frequency. For the locked cavity, when the frequency of this tone was within the feedback bandwidth, the feedback would create a control voltage to compensate for this artificially added noise. However, for frequencies greater than the feedback bandwidth, the feedback could not compensate this. Therefore, for the tones that were well outside the feedback bandwidth, the integrated area of the calibration tone is equal for the locked and unlocked spectra. By comparing the integrated areas of these measured peaks, we have found that the correction factor scales the unlocked power spectral density accurately. Figure 8(a) shows three added modulation peaks of the measured homodyne voltage, both for the unlocked and locked cavity: one within, one just outside, and one well outside the feedback bandwidth. Figure 8(b) shows the total measured power  $P_{\text{cal}}$  of the calibration tones applied. It can be seen that the feedback produces a high-pass filter behavior as expected. For the locked cavity, the powers of the calibration tones well outside the feedback bandwidth show a flat relation, indicating that the feedback did not reduce their noise power. The correction factor was then determined by the difference of the powers at the highest frequency and the corrected unlocked trace was shown. Amending the unlocked data with this calibration has enabled us to compare the unlocked and locked measurements fairly.

- 
- [1] A. M. Den Haan, G. H. Wijts, F. Galli, O. Usenko, G. J. Van Baarle, D. J. Van Der Zalm, and T. H. Oosterkamp, Atomic resolution scanning tunneling microscopy in a cryogen free dilution refrigerator at 15 mK, *Rev. Sci. Instrum.* **85**, 035112 (2014).
- [2] D. Niepce, J. J. Burnett, M. Kudra, J. H. Cole, and J. Bylander, Stability of superconducting resonators: Motional narrowing and the role of Landau-Zener driving of two-level defects, *Sci. Adv.* **7**, eabh0462 (2021).
- [3] R. T. Learn, E. Varga, V. Vadakkumbatt, and J. P. Davis, Precision measurements of the zero-temperature dielectric constant and density of liquid  $^4\text{He}$ , *Phys. Rev. B* **106**, 214509 (2022).
- [4] B. L. Brock, M. P. Blencowe, and A. J. Rimberg, Frequency Fluctuations in Tunable And Nonlinear Microwave Cavities, *Phys. Rev. Appl.* **14**, 054026 (2020).
- [5] C. Müller, J. Lisenfeld, A. Shnirman, and S. Poletto, Interacting two-level defects as sources of fluctuating high-frequency noise in superconducting circuits, *Phys. Rev. B* **92**, 035442 (2015).
- [6] V. Vadakkumbatt, M. Hirschel, J. Manley, T. J. Clark, S. Singh, and J. P. Davis, Prototype superfluid gravitational wave detector, *Phys. Rev. D* **104**, 082001 (2021).
- [7] F. M. Buters, K. Heeck, H. J. Eerkens, M. J. Weaver, F. Luna, S. De Man, and D. Bouwmeester, High- $Q$  nested resonator in an actively stabilized optomechanical cavity, *Appl. Phys. Lett.* **110**, 104104 (2017). ArXiv:1701.04212,
- [8] C. A. Regal, J. D. Teufel, and K. W. Lehnert, Measuring nanomechanical motion with a microwave cavity interferometer, *Nat. Phys.* **4**, 555 (2008). ArXiv:0801.1827,
- [9] T. J. Clark, V. Vadakkumbatt, F. Souris, H. Ramp, and J. P. Davis, Cryogenic microwave filter cavity with a tunability greater than 5 GHz, *Rev. Sci. Instrum.* **89**, 114704 (2018).
- [10] M. De Wit, G. Welker, K. Heeck, F. M. Buters, H. J. Eerkens, G. Koning, H. Van der Mee, D. Bouwmeester, and T. H. Oosterkamp, Vibration isolation with high thermal conductance for a cryogen-free dilution refrigerator, *Rev. Sci. Instrum.* **90**, 015112 (2019).
- [11] C. Lee, H. Jo, C. S. Kang, G. B. Kim, I. Kim, Y. H. Kim, H. J. Lee, and J. So, Vibration mitigation for a cryogen-free dilution refrigerator for the AMoRE-Pilot experiment, *J. Low Temp. Phys.* **193**, 786 (2018).
- [12] S. Kanhirathingal, B. Thyagarajan, B. L. Brock, J. Li, E. Jeffrey, M. P. Blencowe, J. Y. Mutus, and A. J. Rimberg, Feedback Stabilization of the Resonant Frequency in a Tunable Microwave Cavity with Single-Photon Occupancy, *Phys. Rev. Appl.* **18**, 064033 (2022).
- [13] A. Vepsäläinen, R. Winik, A. H. Karamlou, J. Braumüller, A. D. Paolo, Y. Sung, B. Kannan, M. Kjaergaard, D. K. Kim, and A. J. Melville, *et al.*, Improving qubit coherence using closed-loop feedback, *Nat. Commun.* **13**, 1932 (2022).
- [14] R. V. Pound, Electronic frequency stabilization of microwave oscillators, *Rev. Sci. Instrum.* **17**, 490 (1946).
- [15] R. W. P. Drever, J. L. Hall, F. V. Kowalski, J. Hough, G. M. Ford, A. J. Munley, and H. Ward, Laser phase and frequency stabilization using an optical resonator, *Appl. Phys. B* **31**, 97 (1983).
- [16] G. C. Bjorklund, M. D. Levenson, W. Lenth, and C. Ortiz, Frequency modulation (FM) spectroscopy: Theory of line-shapes and signal-to-noise analysis, *Appl. Phys. B* **32**, 145 (1983).
- [17] E. D. Black, An introduction to Pound-Drever-Hall laser frequency stabilization, *Am. J. Phys.* **69**, 79 (2001).
- [18] T. Carmon, T. J. Kippenberg, L. Yang, H. Rokhsari, S. Spillane, and K. J. Vahala, Feedback control of ultra-high- $Q$  microcavities: Application to micro-Raman lasers and microparametric oscillators, *Opt. Express* **13**, 3558 (2005).
- [19] D. Bothner, I. C. Rodrigues, and G. A. Steele, Photon-pressure strong coupling between two superconducting circuits, *Nat. Phys.* **17**, 85 (2021).
- [20] C. A. Potts, E. Varga, V. A. S. V. Bittencourt, S. Viola-Kusminskiy, and J. P. Davis, Dynamical Backaction Magnomechanics, *Phys. Rev. X* **11**, 031053 (2021).
- [21] C. A. Potts, Y. Huang, V. A. S. V. Bittencourt, S. Viola-Kusminskiy, and J. P. Davis, Dynamical backaction evading magnomechanics (2022), arXiv preprint ArXiv:2211.13766.
- [22] X. Zhang, C.-L. Zou, L. Jiang, and H. X. Tang, Cavity magnomechanics, *Sci. Adv.* **2**, e1501286 (2016).
- [23] R.-C. Shen, J. Li, Z.-Y. Fan, Y.-P. Wang, and J. Q. You, Mechanical Bistability in Kerr-Modified Cavity Magnomechanics, *Phys. Rev. Lett.* **129**, 123601 (2022).

- [24] M. Aspelmeyer, T. J. Kippenberg, and F. Marquardt, Cavity optomechanics, *Rev. Mod. Phys.* **86**, 1391 (2014).
- [25] S. R. Peiter, Ph.D. thesis, Delft University of Technology (2022).
- [26] A. Noguchi, R. Yamazaki, M. Ataka, H. Fujita, Y. Tabuchi, T. Ishikawa, K. Usami, and Y. Nakamura, Ground state cooling of a quantum electromechanical system with a silicon nitride membrane in a 3D loop-gap cavity, *New J. Phys.* **18**, 103036 (2016).
- [27] B. M. Brubaker, J. M. Kindem, M. D. Urmey, S. Mittal, R. D. Delaney, P. S. Burns, M. R. Vissers, K. W. Lehnert, and C. A. Regal, Optomechanical Ground-State Cooling in a Continuous and Efficient Electro-Optic Transducer, *Phys. Rev. X* **12**, 021062 (2022).
- [28] R. D. Delaney, M. D. Urmey, S. Mittal, B. M. Brubaker, J. M. Kindem, P. S. Burns, C. A. Regal, and K. W. Lehnert, Superconducting-qubit readout via low-backaction electro-optic transduction, *Nature* **606**, 489 (2022).
- [29] S. A. Fedorov, A. Beccari, A. Arabmoheghi, D. J. Wilson, N. J. Engelsens, and T. J. Kippenberg, Thermal intermodulation noise in cavity-based measurements, *Optica* **7**, 1609 (2020).
- [30] See <https://redpitaya.com/> for information (2023), accessed 2023-03-09.
- [31] D. Rieger, S. Günzler, M. Spiecker, A. Nambisan, W. Wernsdorfer, and I. M. Pop, Fano interference in microwave resonator measurements (2022), arXiv preprint [ArXiv:2209.03036](https://arxiv.org/abs/2209.03036).
- [32] S. Weis, R. Rivière, S. Deléglise, E. Gavartin, O. Arcizet, A. Schliesser, and T. J. Kippenberg, Optomechanically induced transparency, *Science* **330**, 1520 (2010).
- [33] A. H. Safavi-Naeini, T. M. Alegre, J. Chan, M. Eichenfield, M. Winger, Q. Lin, J. T. Hill, D. E. Chang, and O. Painter, Electromagnetically induced transparency and slow light with optomechanics, *Nature* **472**, 69 (2011).
- [34] J. D. Teufel, D. Li, M. Allman, K. Cicak, A. J. Sirois, J. D. Whittaker, and R. W. Simmonds, Circuit cavity electromechanics in the strong-coupling regime, *Nature* **471**, 204 (2011).
- [35] J. D. Teufel, F. Lecocq, and R. W. Simmonds, Overwhelming Thermomechanical Motion with Microwave Radiation Pressure Shot Noise, *Phys. Rev. Lett.* **116**, 013602 (2016).
- [36] J. Suh, A. J. Weinstein, and K. C. Schwab, Optomechanical effects of two-level systems in a back-action evading measurement of micro-mechanical motion, *Appl. Phys. Lett.* **103**, 052604 (2013).
- [37] T. Lindström, J. Burnett, M. Oxborrow, and A. Y. Tzalenchuk, Pound-locking for characterization of superconducting microresonators, *Rev. Sci. Instrum.* **82**, 104706 (2011).
- [38] J. Gao, J. Zmuidzinas, B. A. Mazin, H. G. Leduc, and P. K. Day, Noise properties of superconducting coplanar waveguide microwave resonators, *Appl. Phys. Lett.* **90**, 102507 (2007).
- [39] R. Khatiwada, D. Bowering, A. S. Chou, A. Sonnenschein, W. Wester, D. V. Mitchell, T. Braine, C. Bartram, R. Cervantes, and N. Crisosto, *et al.*, Axion dark matter experiment: Detailed design and operations, *Rev. Sci. Instrum.* **92**, 124502 (2021).
- [40] <https://doi.org/10.5281/zenodo.8263882>.